Physics Letters B 746 (2015) 64–72

Contents lists available at ScienceDirect

Physics Letters B

www.elsevier.com/locate/physletb

Top-quark production in proton–nucleus and nucleus–nucleus collisions at LHC energies and beyond

David d'Enterria [a,*], Krisztián Krajczár [a], Hannu Paukkunen [b,c]

[a] CERN, PH Department, 1211 Geneva, Switzerland
[b] Department of Physics, University of Jyväskylä, P.O. Box 35, FI-40014, University of Jyväskylä, Finland
[c] Helsinki Institute of Physics, P.O. Box 64, FI-00014, University of Helsinki, Finland

ARTICLE INFO

Article history:
Received 23 January 2015
Received in revised form 8 April 2015
Accepted 21 April 2015
Available online 24 April 2015
Editor: J.-P. Blaizot

ABSTRACT

Single and pair top-quark production in proton–lead (p–Pb) and lead–lead (Pb–Pb) collisions at the CERN Large Hadron Collider (LHC) and Future Circular Collider (FCC) energies, are studied with next-to-leading-order perturbative QCD calculations including nuclear parton distribution functions. At the LHC, the pair-production cross sections amount to $\sigma_{t\bar{t}} = 3.4$ μb in Pb–Pb at $\sqrt{s_{\rm NN}} = 5.5$ TeV, and $\sigma_{t\bar{t}} = 60$ nb in p–Pb at $\sqrt{s_{\rm NN}} = 8.8$ TeV. At the FCC energies of $\sqrt{s_{\rm NN}} = 39$ and 63 TeV, the same cross sections are factors of 90 and 55 times larger respectively. In the leptonic final-state $t\bar{t} \to W^+ b\, W^- \bar{b} \to b\bar{b}\,\ell\ell\,\nu\nu$ with $\ell = e^{\pm}, \mu^{\pm}$, after typical acceptance and efficiency cuts, one expects about 90 and 300 top-quarks per nominal LHC-year and $4.7 \cdot 10^4$ and 10^5 per FCC-year in Pb–Pb and p–Pb collisions respectively. The total $t\bar{t}$ cross sections, dominated by gluon fusion processes, are enhanced by 3–8% in nuclear compared to p–p collisions due to an overall net gluon antishadowing, although different regions of their differential distributions are depleted due to shadowing or EMC-effect corrections. The rapidity distributions of the decay leptons in $t\bar{t}$ processes can be used to reduce the uncertainty on the Pb gluon density at high virtualities by up to 30% at the LHC (full heavy-ion programme), and by 70% per FCC-year. The cross sections for single-top production in electroweak processes are also computed, yielding about a factor of 30 smaller number of measurable top-quarks after cuts, per system and per year.

1. Introduction

The multi-TeV energies available at the CERN Large Hadron Collider (LHC) have opened up the possibility to measure, for the first time in heavy-ion collisions, various large-mass elementary particles. After the first observations of the W [1,2] and Z [3,4] bosons, as well as bottom-quark (b-jets) [5], there remains only three Standard Model (SM) elementary particles to be directly measured in nucleus–nucleus collisions: the τ lepton, the Higgs boson, and the top quark. Whereas the τ measurement should be straightforward, that of the Higgs boson is beyond the LHC reach as it requires much larger cross sections and/or luminosities [6], such as those reachable at the proposed Future Circular Collider (FCC) [7] with about seven times larger center-of-mass energies than at the LHC. The study presented here shows, for the first time, that the top-quark – the heaviest elementary particle known – will be produced (singly or in pairs) in sufficiently large numbers to be observed in lead–lead (Pb–Pb) and proton–lead (p–Pb) collisions at the LHC and FCC.

Since the width of the top-quark ($\Gamma_t \approx 2$ GeV) is much larger than the parton-to-hadron transition scale given by $\Lambda_{\rm QCD} \approx 0.2$ GeV, the top-quark is the only coloured particle that decays before its hadronization. Its short lifetime, $\tau_0 = \hbar/\Gamma_t \approx 0.1$ fm/c, implies that the top decays – into a $t \to W\, b$ final-state with a nearly 100% branching ratio [8] – mostly within[1] the strongly-interacting medium, such as the quark–gluon plasma (QGP), formed in nuclear collisions. The large top-quark mass ($m_t \approx 173$ GeV) provides a hard scale for high-accuracy perturbative calculations of its Quantum-ChromoDynamics (QCD) and electroweak production cross sections (next-to-next-to-leading-order, or NNLO, is the cur-

[1] The typical transverse momentum of the produced top quark is usually smaller than its mass, $p_{\rm T} < m_t$, and the Lorentz-boost factor is $\gamma \approx \cosh(y_t)$, where y_t is the t-quark rapidity. At the LHC ($|y_t| < 3$) the Lorentz-dilated mean decay time is $\tau = \gamma\tau_0 \approx 0.1$–1 fm/$c$, and at the FCC ($|y_t| < 5$), $\tau = \gamma\tau_0 \approx 0.1$–7.5 fm/$c$; to be compared with the typical QGP formation time of 1 fm/c, and lifetime of 10–20 fm/c.

* Corresponding author.
E-mail address: dde@cern.ch (D. d'Enterria).

http://dx.doi.org/10.1016/j.physletb.2015.04.044

rent theoretical state-of-the-art [9–11]). At hadron colliders, top quarks are produced either in pairs, dominantly through the strong interaction, or singly through the weak interaction. At the energies considered here, the dominant production channels, as obtained at NLO accuracy with the MCFM code [12], are: (i) gluon–gluon fusion, $g\,g \to t\bar{t} + X$, contributing by 80–95% to the total pair production (the remaining 5–20% issuing from quark–antiquark annihilation), (ii) t-channel single-top electroweak production $q\,b \to q'\,t + X$ (the s-channel process, decreasing with energy, amounts to 5–1.5% of the total single-t cross section), and (iii) associated top plus W-boson, $g\,b \to W\,t + X$, production (increasing with energy, it amounts to 25–50% of the t-channel process).

The theoretical motivations for a dedicated experimental measurement of the top-quark in heavy-ion collisions are varied and include, at least, the following studies:

(i) Constraints on nuclear Parton Distribution Functions (nPDFs). The $t\bar{t}$ cross sections in proton–proton (p–p) collisions can be used to constrain the proton PDFs [13]. In the heavy-ion case, top-pair production probes the nuclear gluon density in an unexplored kinematic regime around Bjorken-x values, $x \approx 2\,m_{\rm t}/\sqrt{s_{\rm NN}} \approx 5 \cdot 10^{-3}$–0.05, and virtualities $Q^2 \approx m_{\rm t}^2 \approx 3 \cdot 10^4$ GeV^2, a region characterized by net positive, albeit small, anti-shadowing corrections. In addition, at the FCC, the b-quark nPDF (in single-top production), and even the top-quark nPDF itself, are generated dynamically by the constituent gluons and become necessary ingredients of the theoretical cross section calculations.

(ii) Heavy-quark energy loss dynamics. The top quark can radiate gluons before its $W\,b$ decay which, given its very-short lifetime, occurs mostly inside the QGP. Medium-induced gluon radiation off light-quarks and gluons, leading to "jet quenching" [14], results in a factor of two reduction of jet yields in Pb–Pb compared to p–p collisions at $\sqrt{s_{\rm NN}} = 2.76$ TeV [15,16]. Although solid theoretical expectations for heavy-quark radiation predict a reduced amount of gluonstrahlung at small angles due to the "dead cone" effect [17], the experimental data somehow unexpectedly shows the same amount of suppression for jets from light-flavours and b-quarks [5]. The relative role of elastic and radiative scatterings on the energy loss of heavy-quarks is an open issue in the field [18,19]. The detailed study of top-quark production in heavy-ion collisions would therefore provide novel interesting insights on the mechanisms of parton energy loss. In addition, the study of boosted top-pairs (with transverse momenta above $p_{\rm T} \approx 1$ TeV) traversing the QGP as a colour-singlet object for a fraction of their time, will allow one to probe the medium opacity at different space–time scales.

(iii) Colour reconnection in the QGP. The top mass, featuring the strongest coupling to the Higgs field, is a fundamental SM parameter with far-reaching implications including the stability of the electroweak vacuum [20]. Currently, one of the dominant $m_{\rm t}$ systematic uncertainties is of theoretical nature and connected to the modelling of the colour connection and QCD interferences between the $t\bar{t}$ production and decay stages, and among the hadronic decay products. Indeed, the colour-flow (through gluon exchanges and/or non-perturbative string overlaps) between the t and $\bar{t}$ quarks, their decayed b-quarks, and the underlying event from multi-parton interactions and beam-remnants surrounding the initial hard scattering [21], results in uncertainties on the reconstructed $m_{\rm t}$ of a few hundred MeV. The amount of top quark interactions with the colour fields stretched among many partons involved in nuclear collisions will be obviously enhanced compared to more elementary systems. Thus, the reconstruction of the top-quark mass in the QGP (assuming its feasibility is not jeopardized by the large b-quark energy loss already observed in the data), or in proton–nucleus interactions, would provide interesting insights in non-perturbative QCD effects on a crucial SM parameter.

In this paper we mostly focus on nPDF constraints through top-pair production in p–Pb and Pb–Pb collisions. We also provide the expected $p_{\rm T}$ reach of top quark spectra at various energies to indicate where boosted final-states can be measured for energy loss studies. The paper is organized as follows. In Section 2 the theoretical setup used is outlined, which is then used to compute the NLO cross sections at the LHC and FCC, and associated yields expected after typical acceptance and efficiency cuts, for top-pair and single-top production, presented in Section 3. Section 4 quantifies the impact on the nuclear PDFs provided by the measurement of the rapidity distributions of the decay leptons from top-quark pairs produced at the LHC and FCC, using a Hessian PDF reweighting technique [22,23]. The main conclusions of the work are summarized in Section 5.

2. Theoretical setup

The top-pair and single-top cross sections are computed at NLO accuracy with the MCFM code [12] (version 6.7) using the NLO CT10 proton PDFs (including its 52 eigenvector sets) [24] corrected for nuclear effects (shadowing, antishadowing and EMC) [25] through the EPS09 nPDFs (including its 30 error sets) for the Pb ion [26]. As our main purpose is to provide estimates for the feasibility of different top-quark measurements in nuclear collisions, we do not discuss here the (subleading) sensitivity of the cross sections to different sets of proton PDFs (nor associated variations of the strong coupling α_s). Also, while there are other nuclear PDF sets available [27–29], we only employ EPS09 here as it is the only nPDF set that is consistent with the dijet measurements in p–Pb collisions at the LHC [30,31] (the data would probably agree also with the latest nPDFs by nCTEQ [32], but these sets are not available at the time of writing this article). We run the following MCFM processes: `141` for $t\bar{t}$ production, `161,166` for single-(anti)top in the t-channel, `171,176` in the s-channel, and `181,186` for associated $t\,W$ production. We note that, at NLO, the theoretical processes defining $t\,W$ production partially overlap with those contributing to top-quark pair production [33]. This is accounted for in our MCFM $t\,W$ cross sections calculations by vetoing the additional emission of a b-jet. The code also properly accounts for the different isospin (u- and d-quark) content of the Pb nucleus, which has a small impact on the electroweak single-top processes.

All numerical results have been obtained using the latest SM parameters for particle masses, widths and couplings [8], and fixing the default renormalization and factorization scales at $\mu = \mu_F = \mu_R = m_{\rm t}$ for $t\bar{t}$ and t-, s-channel single-top, and at $\mu = \mu_F = \mu_R = p_{T,\min;b\text{-jet}} = 50$ GeV for the $t\,W$ processes. The NLO calculations used here reproduce well the cross sections experimentally measured at the LHC in p–p collisions at $\sqrt{s} = 7,\ 8$ TeV for $t\bar{t}$ [34–48], t-channel single-top [46,49–52], and associated $t\,W$ [53–55] production. Incorporation of next-to-NLO corrections [9] would increase the theoretical cross sections, by about 10%, i.e. the so-called K-factor amounts to $K = \sigma_{\rm NNLO}/\sigma_{\rm NLO} \approx 1.10$, and further improve the data-theory agreement. The computed nucleon–nucleon cross sections are scaled by the Pb mass number ($A = 208$) to obtain the p–Pb cross sections, and by $A^2 = 43\,264$ in the Pb–Pb case, as expected for hard scattering processes in nuclear collisions. The uncertainties of the theoretical cross sections are obtained from the values computed using the eigenvector sets of, first, the CT10 and, then, EPS09 PDFs and adding them in

Table 1
Inclusive cross sections for top-pair and single-top (t-channel, s-channel, and tW) production in Pb–Pb and p–Pb collisions at LHC and FCC energies, obtained at NLO accuracy with MCFM. The first uncertainty is due to theoretical scale variations, and the second one to the CT10 and EPS09 PDF errors added in quadrature.

System/Process: (MCFM process)	Top pair ($t\bar{t}$) (141)	Single-top (t-channel) (161,166)	Single-top (s-channel) (171,176)	Single-top (tW) (181,186)
Pb–Pb $\sqrt{s_{\rm NN}} = 5.5$ TeV	$3.40 \pm 0.42 \pm 0.37$ μb	$1.61 \pm 0.05 \pm 0.08$ μb	$110 \pm 4 \pm 6$ nb	$313 \pm 13 \pm 41$ nb
p–Pb $\sqrt{s_{\rm NN}} = 8.8$ TeV	$58.8 \pm 7.1 \pm 3.8$ nb	$21.1 \pm 0.63 \pm 0.63$ nb	$1.09 \pm 0.03 \pm 0.04$ nb	$5.26 \pm 0.21 \pm 0.37$ nb
Pb–Pb $\sqrt{s_{\rm NN}} = 39$ TeV	$302 \pm 33 \pm 12$ μb	$54.6 \pm 1.6 \pm 2.2$ μb	$1.31 \pm 0.05 \pm 0.08$ μb	$24.2 \pm 1.6 \pm 1.3$ μb
p–Pb $\sqrt{s_{\rm NN}} = 63$ TeV	$3.20 \pm 0.35 \pm 0.10$ μb	$518 \pm 16 \pm 17$ nb	$10.9 \pm 0.5 \pm 0.5$ nb	$246 \pm 24 \pm 11$ nb

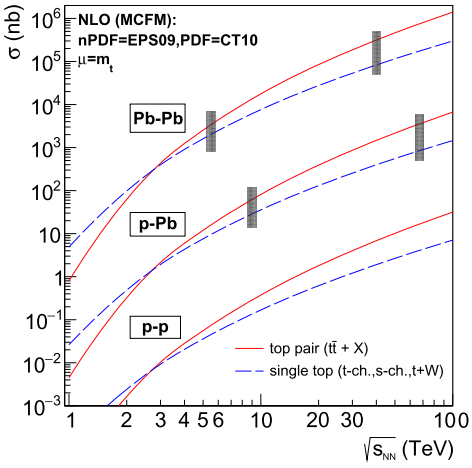

Fig. 1. Total cross sections for top pair and single-top (sum of t-, s-channels plus tW processes) production in Pb–Pb, p–Pb and p–p collisions as a function of c.m. energy. The dashed boxes indicate the nominal nucleon–nucleon c.m. energies, $\sqrt{s_{\rm NN}} = 5.5, 8.8, 39, 63$ TeV, of the heavy-ion runs at the LHC and FCC.

quadrature, as well as by independently varying the renormalization and factorization μ_F and μ_R scales within a factor of two (for the central CT10 and EPS09 set). The PDF and scale uncertainties amount each to 3–10% for $t\bar{t}$ and 3–6% for single top. The scale uncertainties have no impact on the nPDF constraints derived below given that the scale dependence of the nuclear modifications in PDFs around $\mu = m_{\rm t}$ is very mild (see e.g. Fig. 1 in Ref. [56]) and that differences between proton and nuclear PDFs are obtained via ratios of (p–Pb, Pb–Pb)/(p–p) cross sections at the same colliding energy, where those mostly cancel out.

3. Top-pair and single-top cross sections and yields

Table 1 collects the total cross sections, and associated scale and PDF uncertainties, for top-pair and single-top production in p–Pb and Pb–Pb collisions at LHC and FCC energies, obtained as described in the previous section. In the case of $t\bar{t}$ and tW production, a net EPS09 gluon antishadowing in collisions with Pb ions results in an increase of the total production cross sections by about 2–8% compared to those (A-scaled) obtained for p–p collisions using the proton CT10 PDF. For t- and s-channel single-top cross sections, the overall nuclear modifications are quite insignificant, ±2% depending on the energy. Fig. 1 shows the total top-pair and single-top cross sections as a function of collision energy for p–p, p–Pb and Pb–Pb collisions in the range of c.m. energies in the nucleon–nucleon system of $\sqrt{s_{\rm NN}} \approx$ 1–100 TeV. The single-top curves are obtained adding the t-,s-channel and tW cross sections listed in Table 1. In general, top-quark pair production is a factor of two (four) larger than the sum of single top processes at the LHC (FCC). The nominal LHC and FCC energies for p–Pb and Pb–Pb collisions are indicated by dashed boxes in the plot. Going from LHC to FCC, the total cross sections increase by significant factors, ×(55–90) for $t\bar{t}$ and ×(30–40) for single-top.

The impact of nuclear PDF modifications on the yields for a given hard process is usually quantified through the nuclear modification factor $R_{\rm AA}$ given by the ratio of cross sections in nuclear over proton–proton collisions scaled by A or A^2. The theoretical $R_{\rm AA}(y_{t,\bar{t}})$ factors as a function of the rapidity of the produced top and antitop quarks are shown in Fig. 2 for $t\bar{t}$ at LHC (top panels) and FCC (bottom panels) energies. The central curves indicate the result obtained with the central EPS09 set and the grey bands show the corresponding nPDF uncertainties. All the results presented in those, and the following, plots are given in the center-of-mass frame of the colliding species. In general, the $R_{\rm AA}(y_{t,\bar{t}})$ distributions reveal very similar trends for $t\bar{t}$ and single-top (not shown here) processes, although the t-channel and s-channel processes have a factor of two smaller uncertainties, as expected, given that single-top production is dominated by quark-induced processes whose densities in the nucleus are better known than the gluon ones which produce most of the top pairs. At the LHC, for both (single and pair) production mechanisms, the nPDF effects increase the average top-quark distributions at central rapidities by about 10% (antishadowing) while they deplete them by 20% at backward rapidities (also in the forward direction in Pb–Pb) due to the so-called EMC effect at large-x [25] (see also Fig. 4 later). At the FCC, the higher collision energies as well as the larger kinematical coverage assumed for the detectors at this future facility give access to smaller momentum fractions x where EPS09 predicts moderate shadowing even at high virtualities $Q \sim m_t$. This leads to additional suppression at forward rapidities (and also in the backward direction in Pb–Pb).

The cross sections listed in Table 1 and plotted in Fig. 1 are total inclusive ones and do not include the $t \to W\,b$ decays, nor any experimental acceptance/analysis requirements on the final-state particles. The determination of the expected yields at the LHC and FCC requires accounting for top and W-boson decays plus acceptance and reconstruction efficiency losses. The W leptonic branching fractions, $W \to \ell^{\pm}\nu_{\ell}$ (with $\ell = {\rm e}, \mu, \tau$), amount to 1/9 for each lepton flavour, the other 2/3 being due to W dijet (quark–antiquark) decays. In this work we will only consider leptonic W decays characterized by a final-state with an isolated electron or muon plus missing transverse energy ($\not{E}_{\rm T}$) from the neutrino, because the W dijet-decays are much more difficult to reconstruct in the large background of heavy-ion collisions, and also potentially subject to parton energy loss effects (although they could be certainly tried in the "cleaner" p–Pb environment). For the top-pairs measurement, $t\bar{t} \to W^+ b\, W^- \bar{b} \to b\,\bar{b}\,\ell\ell\,\nu\nu$, the combination of electron and muon decays for both W-bosons ($ee, \mu\mu, e\mu, \mu e$) reduces the total cross sections by a factor[2] of $\mathcal{B}_{\ell\ell} = 4/9^2 \approx 1/20$. For the single-top case, we will only consider the yields for associated tW production which shares a characteristic final-state signature, $tW \to W\,b\,W \to b\,\ell\ell\,\nu\nu$, very similar to that of top-pair production. Indeed, the experimental observation of t-channel (let alone the much more suppressed s-channel) single-top, with one

[2] Including also $e^{\pm}$ and $\mu^{\pm}$ from leptonic tau-decays in the $t\bar{t} \to e\tau, \mu\tau, \tau\tau + \not{E}_{\rm T}$ final-states would decrease the corresponding branching ratio only to $\mathcal{B}_{\ell\ell} \approx 1/16$.

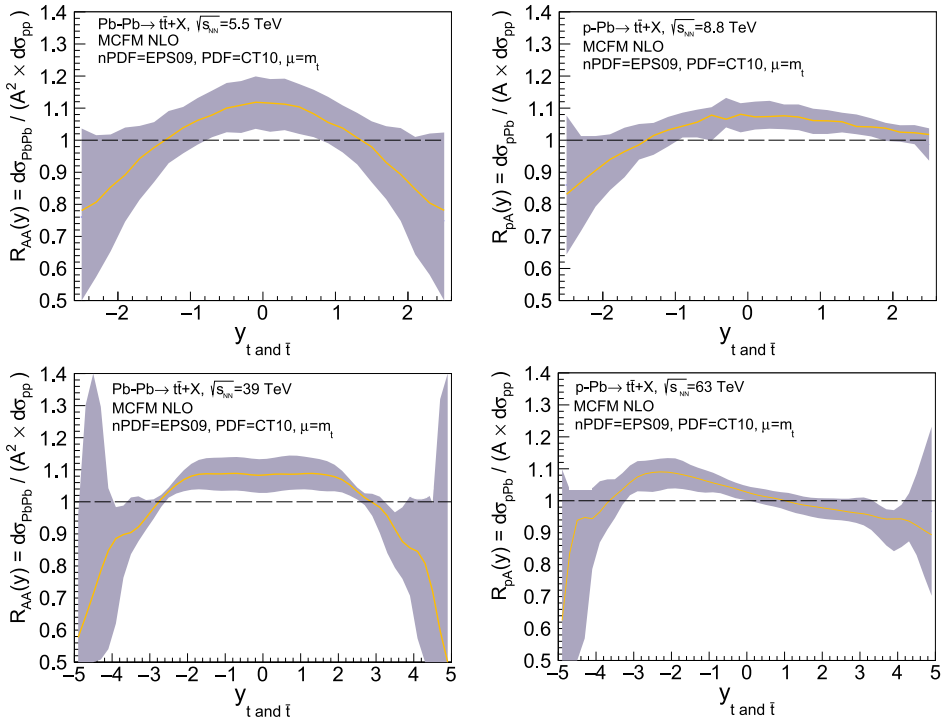

Fig. 2. Theoretical nuclear modification factor as a function of rapidity of the individual top and antitop quarks in $t\bar{t}$ production in Pb–Pb (left panels) and p–Pb (right panels) at $\sqrt{s_{\rm NN}} = 5.5, 8.8$ TeV (LHC, top panels) and 39, 63 TeV (FCC, bottom panels), computed at NLO accuracy with MCFM. The central curve indicates the result obtained with the central EPS09 parametrization and the grey band the corresponding nPDF uncertainty.

Table 2
List of analysis cuts on single $p_{\rm T}$ and η for b-jets and isolated leptons $\ell = e^{\pm}, \mu^{\pm}$, and on the neutrinos $\not{E}_{\rm T}$, typically employed in top-pair ($t\bar{t} \to b\bar{b}\ell\ell\nu\nu$) [35,38] and single-top plus W-boson ($tW \to b\ell\ell\nu\nu$) [54] measurements in fully-leptonic final-states in p–p collisions at the LHC, applied in our generator-level studies.

Analysis cuts
b-jets (anti-$k_{\rm T}$ algorithm with $R = 0.5$): $p_{\rm T} > 30$ GeV; $\|\eta\| < 2.5$ (LHC), 5 (FCC)
charged leptons $\ell(R_{\rm isol} = 0.3)$: $p_{\rm T} > 20$ GeV; $\|\eta\| < 2.5$ (LHC), 5 (FCC)
neutrinos: $\not{E}_{\rm T} > 40$ GeV

less charged lepton and neutrino, is much more challenging on top of the expected large W, Z+jets background (in Pb–Pb, at least, although it should be feasible in p–Pb collisions).

In order to compute the expected number of top-quarks measurable at the LHC and FCC, we include in the MCFM generator-level calculations the typical analysis and fiducial requirements for b-jets, charged leptons, and missing transverse energy from the unidentified neutrinos, used in similar p–p measurements at the LHC [35,38,54]. Although some of these p–p experimental requirements may seem optimistic for the more complex environment encountered in heavy-ion collisions, they are validated by future experimental projections of the CMS Collaboration [57]. In the case of FCC, we extend the pseudorapidity coverage for charged-lepton tracking and b-jet secondary vertexing from the LHC range of $|\eta| = 2.5$, to $|\eta| = 5$. The details of all selection criteria are given in Table 2. We reconstruct the b-jets with the anti-$k_{\rm T}$ jet clustering algorithm [58] with distance parameter $R = 0.5$, and we require the high-$p_{\rm T}$ charged lepton to be separated from the closest b-jet within an (η, ϕ) isolation radius of $R_{\rm isol} = 0.3$.

The combination of all analysis cuts listed in Table 2 results in total acceptances of order $\mathcal{A}_{t\bar{t}} \approx \mathcal{A}_{tW} \approx 40\%$ (50%) for $t\bar{t}$ and tW measurements at the LHC (FCC). In addition, one has to account for experimental b-jet tagging efficiencies, which we conservatively take of the order of 50% as determined in Pb–Pb collisions at $\sqrt{s} = 2.76$ TeV [5]. For single-top, this results in an extra $\varepsilon_{tW} \approx 0.5$ reduction of the measured yields. In the $t\bar{t}$ case, in order to tag the event as such, one usually only requires a single b-jet (out of the two produced) to be identified, and thus the associated efficiency is larger: $\varepsilon_{t\bar{t}} \approx 1 - (1 - 0.5)^2 = 0.75$. The combination of acceptance, analysis requirements, and efficiency losses results in an overall efficiency factor of $\mathcal{A}_{t\bar{t}} \times \varepsilon_{t\bar{t}} \approx 30\%$ (40%) for the final $t\bar{t}$ yields[3] at the LHC (FCC). The same factor for tW production is $\mathcal{A}_{tW} \times \varepsilon_{tW} \approx 20\%$ (25%) at the LHC (FCC). Possible backgrounds, mostly from W, Z+jets, WZ, and ZZ production sharing similar final-state signatures as both top-quark production processes, can be minimized by applying dedicated jet-veto requirements and/or extra criteria on the invariant masses of the two high-$p_{\rm T}$ leptons, e.g. away from the Z boson peak ($|m_Z - m_{\ell\ell}| > 15$ GeV). We do not directly compute the impact of such backgrounds here as the applied analysis cuts already reduce them to a manageable level according to the existing p–p measurements. In particular, the application of $m_{\ell\ell}$ cuts would reduce the visible yields by an extra 10% which is, however, compensated by the fact that our NLO calculations need to be scaled by about the same amount to match the current p–p data (and NNLO predictions). We note also that, despite the larger hadronic backgrounds in nuclear collisions, the instantaneous luminosities in the heavy-ion operation mode at the LHC (and FCC) result in a very small event pileup, at variance with the p–p case, and make the top-quark measurements accessible without the complications from overlapping nuclear collisions occurring simultaneously in the same bunch crossing.

[3] We note that, in the Pb–Pb case, parton energy loss effects, which can bring the b-jet below the $p_{\rm T}$ threshold criterion ($p_{\rm T} > 30$ GeV) and result in an additional inefficiency to tag the $t\bar{t}$ event, are unlikely to affect *both* b-jets at the same time. Indeed, for simple geometrical reasons if one top-quark is produced and decays through the denser region, the other one emitted back-to-back will go through a thinner medium layer and its associated b-jet will be tagged with our considered probability.

Table 3
Expected number of top + antitop quarks per run, after typical acceptance and efficiency losses, for top-pair and tW single-top measurements in fully-leptonic final-states in p–Pb and Pb–Pb collisions at LHC and FCC energies for the nominal per-year luminosities quoted.

System	$\sqrt{s}$	$\mathcal{L}_{\rm int}$	Number of top + antitop quarks $t\bar{t} \to b\bar{b}\,\ell\ell\,\nu\nu$	Number of top + antitop quarks $tW \to b\,\ell\ell\,\nu\nu$
Pb–Pb	5.5 TeV	1 nb^{-1}	90	3
p–Pb	8.8 TeV	0.2 pb^{-1}	300	10
Pb–Pb	39. TeV	5 nb^{-1}	47 000	1300
p–Pb	63. TeV	1 pb^{-1}	100 000	2600

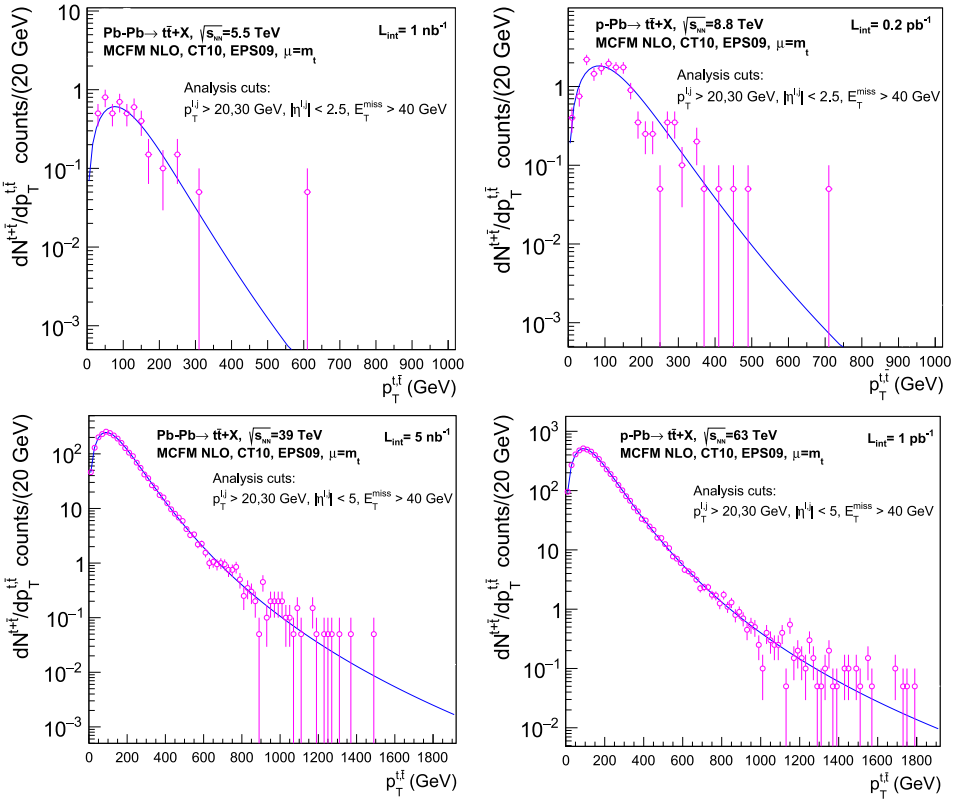

Fig. 3. Expected top-quark $p_{\rm T}$ distributions, $dN^{t+\bar{t}}/dp_{\rm T}^{t,\bar{t}}$, in Pb–Pb (left panels) and p–Pb (right panels) in the fully-leptonic decay modes at $\sqrt{s_{\rm NN}} = 5.5, 8.8$ TeV (LHC, top panels) and 39, 63 TeV (FCC, bottom panels) after acceptance and efficiency cuts. The curves are a fit to the underlying MCFM distribution. The markers indicate pseudodata corresponding to the luminosities listed in Table 3.

The expected total number of top-quarks (adding the t and $\bar{t}$ values) produced in Pb–Pb and p–Pb in one year at the nominal luminosities for each colliding system, obtained via $\mathcal{N} = \sigma \cdot \mathcal{B}_{\ell\ell} \cdot \mathcal{L}_{\rm int} \cdot \mathcal{A} \cdot \varepsilon$, are listed in Table 3. The number of visible single tops in tW processes is smaller by a factor of ∼30 compared to those from $t\bar{t}$ production, due to a combination of causes: lower cross sections, smaller reconstruction efficiencies, and only one top-quark per event. At the LHC, we expect about 100 and 300 top-quarks measurable in the fully leptonic decays from $t\bar{t}$-pairs and tW processes in Pb–Pb and p–Pb respectively. For comparison, the CDF and D0 experiments reconstructed less than 100 top-quarks (in all decays channels) during the full Run-1 operation at Tevatron. At the end of the LHC heavy-ion programme, with $\mathcal{L}_{\rm int} \approx 10$ nb^{-1} (1 pb^{-1}) integrated in Pb–Pb (p–Pb), about 2.5 thousand (fully-leptonic) (anti)top-quarks should have been measured individually by the CMS and ATLAS experiments. The corresponding visible yields at the FCC are about 300 times larger, reaching 5×10^4 and 10^5 top-quarks per year in Pb–Pb and p–Pb collisions respectively.

In order to provide an idea of the top-quark $p_{\rm T}$ reach accessible in the different measurements listed in Table 3, we have also computed the expected $t, \bar{t}$ transverse-momentum distributions in Pb–Pb and p–Pb collisions, after all acceptance and efficiency criteria applied (Fig. 3). The maximum top-quark $p_{\rm T}$ experimentally measurable per LHC (FCC) year will be around $p_{\rm T} \sim 300$ (1500) GeV for Pb–Pb, and $p_{\rm T} \sim 500$ (1800) GeV for p–Pb. Given the limited LHC top-quark statistics, the study of boosted-tops will be thus only accessible at the Future Circular Collider.

4. Constraints on nuclear PDFs from $t\bar{t}$ production

As aforementioned, 80–95% of the total pair production at LHC–FCC comes from gluon–gluon fusion processes and, thus, $t\bar{t}$ cross sections can be used to constrain the relatively badly-known gluon densities in the Pb nucleus. In this section we quantify the impact that top-quark measurements at the LHC and FCC would have on better constraining the nuclear PDFs through the so-called Hessian PDF reweighting technique [22,23]. Such PDF reweighting procedure is based on the fact that the error sets $\{f\}_k^{\pm}$ defined in Hessian PDF-fits correspond to a certain increment $\Delta\chi^2$ ($\Delta\chi^2 = 50$ for EPS09) of the global "goodness-of-fit" χ^2 function whose minimum χ_0^2 is achieved with the central set $\{f\}_0$. The error sets thereby constitute a parametrization of the orig-

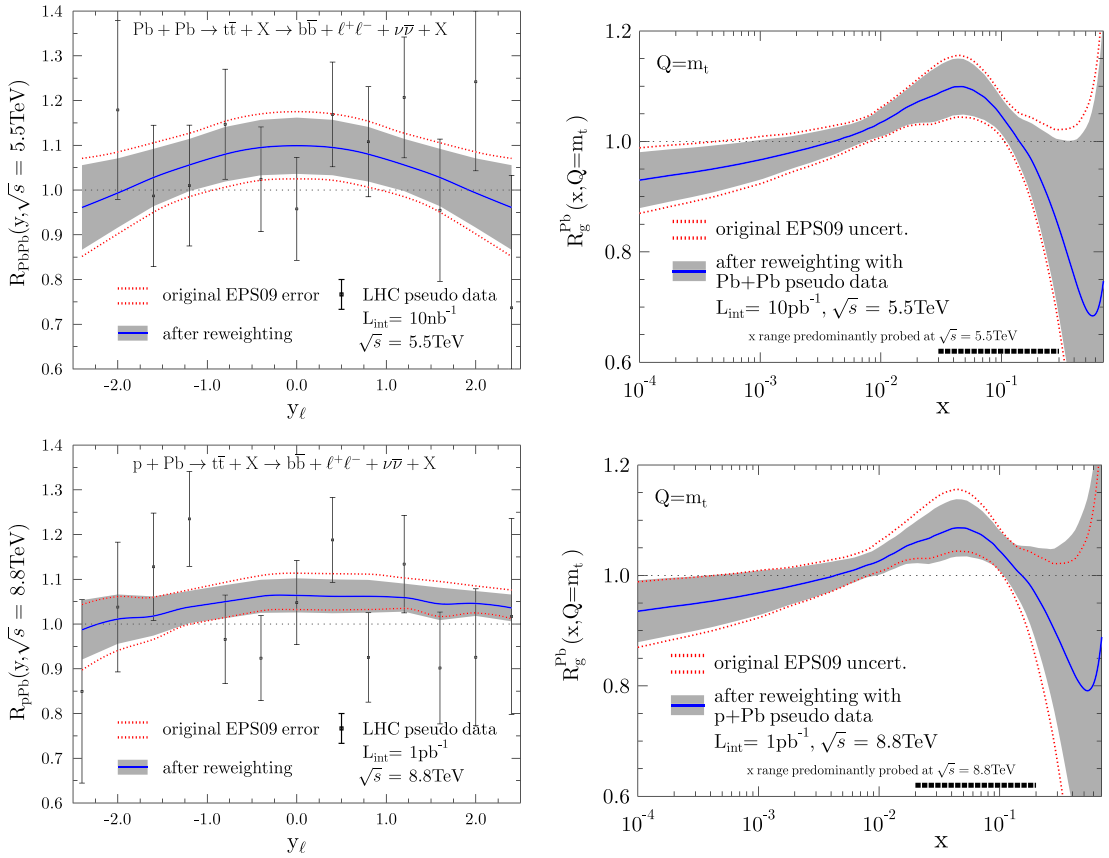

Fig. 4. Impact on the nuclear glue of $t\bar{t}$ (pseudo)data for the full LHC heavy-ion programme. Left: Nuclear modification factor for $t\bar{t}$ decay-leptons as a function of rapidity, $R_{\rm PbPb}(y_\ell)$, obtained for Pb–Pb at $\sqrt{s_{\rm NN}} = 5.5$ TeV (top) and p–Pb at $\sqrt{s_{\rm NN}} = 8.8$ TeV (bottom) compared to predictions computed with EPS09: current nPDF set (region enclosed by the red dotted lines) and after pseudodata-reweighting (blue curve plus grey band). Right: Ratio of nuclear-over-proton gluon densities, $R_{\rm g}^{\rm Pb}$ evaluated at $Q = m_{\rm t}$, for the original EPS09 (band enclosed by red dotted lines) and for the reweighted EPS09 (blue curve with grey band) for Pb–Pb (top) and p–Pb (bottom). (For interpretation of the references to colour in this figure legend, the reader is referred to the web version of this article.)

inal χ^2 function which can be taken advantage of in order to determine the associated PDF uncertainty after adding new experimental datasets. More precisely, the Hessian method [59] for determining the PDF errors writes the response of the original χ^2 function to fit-parameter variations δa_i as

$$\chi^2\{a\} - \chi^2_0 \approx \sum_{i,j} \delta a_i H_{ij} \delta a_j = \sum_k z_k^2, \tag{1}$$

where the Hessian matrix $H_{ij} = (1/2)\partial^2\chi^2/(\partial a_i \partial a_j)$ is diagonalized in the last step. The PDF error sets $\{f\}^{\pm}_k$ are then defined by $z_i(\{f\}^{\pm}_k) = \pm\sqrt{\Delta\chi^2}\delta_{ik}$. The impact of including new experimental data can now be computed by considering a function

$$\chi^2_{\rm new} \equiv \sum_k z_k^2 + \sum_{i,j} [T_i(z) - D_i] C^{-1}_{ij} \left[T_j(z) - D_j\right], \tag{2}$$

where D_i denote the ith new data-point and C is the covariance matrix that encodes the experimental uncertainties. The corresponding theoretical values are denoted by T_i and they depend on the PDFs. To first approximation, the z dependence of each T_i is given by

$$T_i(z) \approx T_i(0) + \sum_k \frac{T_i(z^+_k) - T_i(z^-_k)}{2} w_k, \tag{3}$$

where $w_k \equiv z_k/\sqrt{\Delta\chi^2}$, $T_i(0)$ is the theory value computed with the central set $\{f\}_0$, and $T_i(z^{\pm}_k)$ is the theory value evaluated with the error set $\{f\}^{\pm}_k$. Inserting Eq. (3) into Eq. (2) and requiring $\partial\chi^2_{\rm new}/\partial w_k = 0$ for all k, one finds the condition $w^{\rm min}_k = -\sum_i B^{-1}_{ki} a_i$ for the minimum of $\chi^2_{\rm new}$, where $B_{kn} = \sum_{i,j} D_{ik} C^{-1}_{ij} D_{jn} + \Delta\chi^2\delta_{kn}$, $a_k = \sum_{i,j} D_{ik} C^{-1}_{ij} \left[T_j(0) - D_j\right]$, and $D_{ik} = \left(T_i(z^+_k) - T_i\left(z^-_k\right)\right)/2$. The new theory values $T^{\rm new}_i$ are obtained directly from Eq. (3) with $w_k = w^{\rm min}_k$, and the corresponding new central set of PDFs $\{f^{\rm new}\}_0$ by replacing T_i with the PDFs, $T_i \to f^{\rm new}(x, Q^2)$. To find the new PDF error sets $\{f^{\rm new}\}^{\pm}_k$, we rewrite Eq. (2) as

$$\chi^2_{\rm new} - \chi^2_{\rm new}|_{\mathbf{w}=\mathbf{w}^{\rm min}} = \sum_{i,j} \delta w_i B_{ij} \delta w_j = \sum_k v_k^2, \tag{4}$$

where $\delta w_i = w_i - w^{\rm min}_i$, and in the last step the matrix B is being diagonalized. The new PDF error sets $\{f^{\rm new}\}^{\pm}_k$ can be then defined exactly as earlier by $v_i(\{f^{\rm new}\}^{\pm}_k) = \pm\sqrt{\Delta\chi^2}\delta_{ik}$. The procedure sketched above was proven in Ref. [23] to be consistent with the Bayesian reweighting method introduced originally in Ref. [60] and further confirmed more recently in Ref. [61].

To mimic a realistic experimental situation, we generate sets of pseudodata for nuclear-modification factors $R_{\rm pPb}$ and $R_{\rm PbPb}$ – i.e. for the ratios of cross sections obtained with EPS09 nPDFs over those obtained with the CT10 proton PDFs – corresponding to the LHC and FCC scenarios discussed in the previous section. As noted earlier, the *total* $t\bar{t}$ production cross section is expected to undergo only a mild increase due to nuclear effects in the nPDFs, and it may be challenging to resolve such an effect from overall normalization uncertainties. Thus, the total $t\bar{t}$ cross sections are not expected to have as large impact as they have on the absolute free proton

PDFs [13]. In order to get better constraints on the nPDFs differential cross sections are thus needed. For this purpose, we use the distributions of leptonic top-decay products, which are unaffected by final-state interactions in the strongly-interacting matter produced in nuclear collisions. Here, we concentrate on the measurement of $t\bar{t}$ pairs via the $t\bar{t} \to b\bar{b} + \ell^+\ell^- + \nu\bar{\nu}$ decay channel, binned in the charged lepton rapidity dN_ℓ/dy_ℓ with $\ell = \mathrm{e}, \mu$. The baseline for the pseudodata is taken from the nuclear modification factors computed with the central set of EPS09 in the previous section. The expected number of events $N(\Delta y_i)$ in each rapidity bin Δy_i are computed by

$$N(\Delta y_i) = N_{\mathrm{total}} \times \frac{\sigma(y_i \in \Delta y)}{\sigma_{\mathrm{total}}}, \tag{5}$$

where N_{total} is the total number of events expected after acceptance and efficiency losses for each system[4] listed in Table 3, $\sigma(y_i \in \Delta y)$ is the cross section within rapidity bin Δy_i, and σ_{total} is the total cross section within the acceptance. The statistical uncertainty is then taken to be $\delta_i^{\mathrm{stat}} = T_i^{\mathrm{EPS09}}\sqrt{1/N(\Delta y_i)}$ to which we add in quadrature a constant $\pm 5\%$ systematic error ($\delta_i^{\mathrm{syst}} = 0.05 \times T_i^{\mathrm{EPS09}}$), such that the total uncorrelated error is $\delta_i^{\mathrm{uncorr}} = \sqrt{(\delta_i^{\mathrm{stat}})^2 + (\delta_i^{\mathrm{syst}})^2}$. The overall normalization error is taken to be 5% ($\delta_i^{\mathrm{norm}} = 0.05 \times T_i^{\mathrm{EPS09}}$). Systematic uncertainties of this order are realistic as the corresponding p–p measurements at the LHC [38,39] have already reached a better precision. In addition, partial cancellations of systematic uncertainties common to p–p, p–Pb, and Pb–Pb measurements are expected in a careful experimental determination of R_{pPb} and R_{PbPb}. The statistical precision of the p–p baseline data, taken at slightly different center-of-mass energies, is also much better than that of the p–Pb and Pb–Pb measurements, and the additional theory uncertainty for energy-dependent corrections of the reference cross sections (e.g. to go from $\sqrt{s} = 8$ TeV in p–p to $\sqrt{s_{\mathrm{NN}}} = 8.8$ TeV in p–Pb at the LHC) are small [62]. Each pseudodata point D_i is then computed from the baseline values T_i^{EPS09} and from the estimated uncorrelated and normalization errors by $D_i = \left(T_i^{\mathrm{EPS09}} + \delta_i^{\mathrm{uncorr}} r_i + \delta_i^{\mathrm{norm}} r^{\mathrm{norm}}\right)$, where r_i and r^{norm} are random numbers from a Gaussian distribution of variance one centered around zero. The elements of the covariance matrix C are computed as $C_{ij} = \left[\delta_i^{\mathrm{uncorr}}\delta_j^{\mathrm{uncorr}}\delta_{ij} + \delta_i^{\mathrm{norm}}\delta_j^{\mathrm{norm}}\right]$ [63].

In the original EPS09 analysis [26], the inclusive pion data measured at RHIC [64] was given an additional weight factor of 20 in the χ^2-function in order to enhance the constraints on the badly known gluon densities from nuclear deep-inelastic and fixed-target Drell–Yan data alone. As both the pion data and the top quark production considered here, are mostly sensitive to nuclear gluon PDFs, we rescale the covariance matrix equally by $C \to C/20$ when performing the reweighting. This compensates for the large weight given for the RHIC pion data and should lead to a more realistic estimate of the impact that the top-quark measurements would have if directly included into the EPS09 fit. After finding the new theory values T_i^{new} through the reweighting procedure, the optimum overall shift (originating from the allowed uncertainty in normalization) is found by solving the multiplicative factor f from the χ^2 contribution of the new data (see e.g. Ref. [63]):

$$\sum_{i,j}\left[T_i^{\mathrm{new}} - D_i\right] C_{ij}^{-1}\left[T_j^{\mathrm{new}} - D_j\right]$$

$$= \min\left\{\sum_i \left[\frac{T_i^{\mathrm{new}} - D_i - f\delta_i^{\mathrm{norm}}}{\delta_i^{\mathrm{uncorr}}}\right]^2 + f^2\right\}. \tag{6}$$

In the results presented below, the resulting shift $f\delta_i^{\mathrm{norm}}$ has been applied on the data points.

The results of the nPDF reweighting procedure are presented first for LHC energies in Fig. 4 for Pb–Pb (top) and p–Pb (bottom) collisions. The nuclear modifications for the decay leptons are somewhat less pronounced in comparison to the top distributions themselves (Fig. 2) due to the smoothing brought about by the additional phase–space integrations related to the top-quark decays. The estimated statistical errors are generally of the order of 10% and are foreseen to dominate over the predicted systematic uncertainties. These pseudodata probe the nuclear PDFs predominantly in the range $0.03 \lesssim x \lesssim 0.3$ at $\sqrt{s} = 5.5$ TeV, and $0.02 \lesssim x \lesssim 0.2$ at $\sqrt{s} = 8.8$ TeV, as inferred from our MCFM calculations. In both cases the pseudodata are found to have only a moderate impact on the EPS09 gluon density.[5] This is predominantly due to the rather low foreseen statistics and the rapidity interval covered, which makes especially $R_{\mathrm{pPb}}(y_\ell)$ somewhat flat within the acceptance. Consequently, even the overall normalization alone can mimic the effects of nuclear PDFs thereby reducing the obtainable constraints. The new error bands in Figs. 4 are both around 10% narrower than the original EPS09 ones. Combining the p–Pb and Pb–Pb measurements and assuming independent data samples available from both the CMS and ATLAS Collaborations, the total impact of $t\bar{t}$ production on the large- and mid-x nuclear gluons could reach 30% (with the full LHC luminosity). Such a modest improvement will most likely be overpowered by the constraints offered by the inclusive jet and dijet data from the LHC p–Pb run(s) [31].

The results of repeating the reweighting procedure with the FCC pseudodata are shown in Fig. 5 for Pb–Pb (top) and p–Pb (bottom) collisions respectively. Although the foreseen FCC per-year integrated luminosities are similar to those expected for the *full* LHC heavy-ion programme, the production cross sections being a factor $\times$(55–90) above the LHC expectations (Table 3) significantly increase the expected top-quark yields thereby reducing the statistical uncertainties. Indeed, in our FCC scenario the systematic uncertainties dominate. The reduced uncertainties as well as the wider kinematic reach at the FCC make the impact of these pseudodata on EPS09 clearly larger than that expected at the LHC. The constraints also reach lower values of x, the dominant x region being $5 \times 10^{-4} \lesssim x \lesssim 3 \times 10^{-1}$ at $\sqrt{s} = 39$ TeV, and $2 \times 10^{-4} \lesssim x \lesssim 2 \times 10^{-1}$ at $\sqrt{s} = 63$ TeV. The addition of the nuclear $t\bar{t}$ results shown in Fig. 5 would allow one to decrease the gluon density uncertainty by up to 50% in some regions. Unlike in p–Pb collisions, in the Pb–Pb case the nuclear effects coming from small-x (shadowing) and large-x (EMC effect) cannot be distinguished since they are essentially multiplied at large $|y_\ell|$. In this case, the new constraints tend to affect more the part that is originally less constrained, the high-x gluons. That is, while the probed region in x is very similar in our p–Pb and Pb–Pb scenarios, the p–Pb collisions are foreseen to provide more varied nPDF constraints. Combination of p–Pb and Pb–Pb data, plus assumption of two independent experiments measuring the spectra, would result in an overall reduction of up to 70% with just one year of integrated luminosity.

[4] For the LHC, we consider the total luminosity to be accumulated during the *full* heavy-ion programme, which is a factor of 10 (5) higher than the nominal per-year luminosities quoted for Pb–Pb (p–Pb).

[5] As the Q^2 dependence of $R_g^{\mathrm{Pb}}(x, Q^2)$ is rather mild for $Q^2 \gtrsim 10$ GeV^2 [56], the plots at $Q^2 = m_t^2$ are representative for most practical applications.

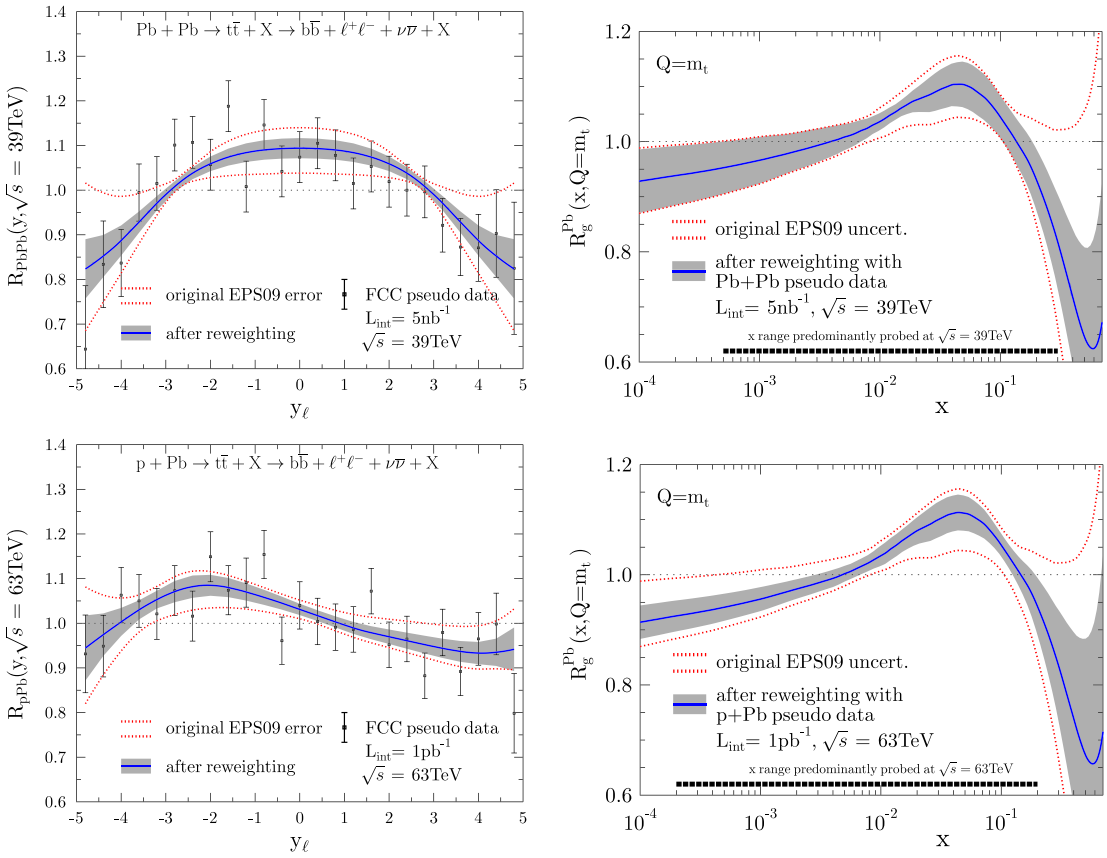

Fig. 5. As Fig. 4 but for the case of Pb–Pb (top) and p–Pb (bottom) per FCC-year pseudodata.

5. Conclusions

The study presented here has shown, for the first time, that top quarks produced in pairs via (mostly) gluon–gluon fusion, or singly in electroweak processes, are clearly observable in p–Pb and Pb–Pb collisions at the energies of the CERN LHC and Future Circular Collider (FCC). The corresponding cross sections have been computed at NLO accuracy with the MCFM code including the CT10 free proton PDFs and nuclear modifications parametrized with the EPS09 nPDF. At the LHC, the pair-production cross sections are $\sigma_{t\bar{t}} = 3.4$ μb for Pb–Pb at $\sqrt{s_{\rm NN}} = 5.5$, and $\sigma_{t\bar{t}} = 60$ nb for p–Pb at $\sqrt{s_{\rm NN}} = 8.8$ TeV. At the FCC energies of $\sqrt{s_{\rm NN}} = 39,\ 63$ TeV, the same cross sections are factors of 90 and 55 times larger respectively. The total $t\bar{t}$ cross sections are enhanced by 3–8% in nuclear compared to p–p collisions at the same c.m. energies, due to an overall net gluon antishadowing, although different regions of the top-quark differential distributions are depleted due to shadowing and EMC-effect corrections. The total cross sections for single-top, including the sum of t- and s-channels plus associated tW processes, are a factor of two (four) smaller than that for top-pair production at the LHC (FCC) and feature minimal nuclear modifications (±2% depending on the energy).

After applying typical acceptance and efficiency cuts in the leptonic ($\ell = e^{\pm}, \mu^{\pm}$) final-state, $t\bar{t} \to W^+ b\, W^- \bar{b} \to b\,\bar{b}\,\ell\ell\,\nu\nu$, one expects about 100 and 300 (anti)top-quarks per LHC-year and 5×10^4 and 10^5 per FCC-year at the nominal luminosities in Pb–Pb and p–Pb collisions respectively. At the end of the LHC heavy-ion programme, with $\mathcal{L}_{\rm int} \approx 10$ nb^{-1}, 1 pb^{-1} integrated Pb–Pb and p–Pb luminosities, about 2.5 thousand (fully-leptonic) $t,\bar{t}$-quarks should have been measured individually by the CMS and ATLAS experiments. The number of visible single-top quarks produced in association with a W boson, in the similar $tW \to WbW \to b\,\ell\ell\,\nu\nu$ final state, is lower by a factor of about 30 compared to $t\bar{t}$ production, due to the combination of lower cross sections, smaller reconstruction efficiencies, and only one top-quark per event.

The proposed top-quark measurements at the LHC and FCC would not only constitute the first observation in nuclear collisions of the heaviest-known elementary particle, but would open up interesting novel physics opportunities such as constraints of nuclear parton densities in an unexplored kinematic range, studies of the dynamics of heavy-quark energy loss in the QGP, and colour-reconnection effects on the top-quark mass. We have, in particular, quantified the impact on the nuclear PDFs of the rapidity-differential distributions of the decay leptons from top-quark pairs, through the Hessian reweighting technique, finding that the data can be used to reduce the uncertainty on the Pb gluon density at high virtualities by up to 30% using the full LHC heavy-ion programme, and by about 70% with just one FCC-year.

Acknowledgements

We are grateful to Carlos Salgado for early discussions on this work, and to Andrea Dainese and Martijn Mulders for feedback on the manuscript. K.K. acknowledges partial financial support from the Hungarian Scientific Research Fund (K 109703).

References

[1] S. Chatrchyan, et al., CMS Collaboration, Phys. Lett. B 715 (2012) 66, arXiv:1205.6334 [nucl-ex].
[2] G. Aad, et al., ATLAS Collaboration, arXiv:1408.4674 [hep-ex].
[3] S. Chatrchyan, et al., CMS Collaboration, Phys. Rev. Lett. 106 (2011) 212301, arXiv:1102.5435 [nucl-ex];
S. Chatrchyan, et al., CMS Collaboration, arXiv:1410.4825 [nucl-ex].
[4] G. Aad, et al., ATLAS Collaboration, Phys. Rev. Lett. 110 (2013) 022301, arXiv:1210.6486 [hep-ex].

[5] S. Chatrchyan, et al., CMS Collaboration, Phys. Rev. Lett. 113 (2014) 132301, arXiv:1312.4198 [nucl-ex].
[6] D. d'Enterria, C. Loizides, in preparation.
[7] N. Armesto, et al., arXiv:1407.7649 [nucl-ex].
[8] J. Beringer, et al., PDG Collaboration, Phys. Rev. D 86 (2012) 010001.
[9] M. Czakon, A. Mitov, J. High Energy Phys. 1301 (2013) 080, arXiv:1210.6832 [hep-ph].
[10] N. Kidonakis, Phys. Part. Nucl. 45 (2014) 714, arXiv:1210.7813 [hep-ph].
[11] M. Czakon, P. Fiedler, A. Mitov, Phys. Rev. Lett. 110 (2013) 252004, arXiv:1303.6254 [hep-ph].
[12] J.M. Campbell, R.K. Ellis, Nucl. Phys. B, Proc. Suppl. 205–206 (2010) 10, arXiv:1007.3492 [hep-ph], http://mcfm.fnal.gov.
[13] M. Czakon, M.L. Mangano, A. Mitov, J. Rojo, J. High Energy Phys. 1307 (2013) 167, arXiv:1303.7215 [hep-ph].
[14] D. d'Enterria, in: Landolt-Boernstein, vol. 1-23A, Springer Verlag, 2010, arXiv:0902.2011 [nucl-ex].
[15] S. Chatrchyan, et al., CMS Collaboration, Phys. Rev. C 84 (2011) 024906, arXiv:1102.1957 [nucl-ex];
S. Chatrchyan, et al., CMS Collaboration, Phys. Lett. B 712 (2012) 176, arXiv:1202.5022 [nucl-ex].
[16] G. Aad, et al., ATLAS Collaboration, Phys. Rev. Lett. 105 (2010) 252303, arXiv:1011.6182 [hep-ex];
G. Aad, et al., ATLAS Collaboration, arXiv:1411.2357 [hep-ex].
[17] Y.L. Dokshitzer, V.A. Khoze, S.I. Troian, J. Phys. G 17 (1991) 1602;
Y.L. Dokshitzer, D.E. Kharzeev, Phys. Lett. B 519 (2001) 199, arXiv:hep-ph/0106202.
[18] P. Gossiaux, J. Aichelin, T. Gousset, Prog. Theor. Phys. Suppl. 193 (2012) 110, arXiv:1201.4038 [hep-ph].
[19] M. Djordjevic, M. Djordjevic, Phys. Lett. B 734 (2014) 286, arXiv:1307.4098 [hep-ph].
[20] S. Alekhin, A. Djouadi, S. Moch, Phys. Lett. B 716 (2012) 214, arXiv:1207.0980 [hep-ph].
[21] P.Z. Skands, D. Wicke, Eur. Phys. J. C 52 (2007) 133, arXiv:hep-ph/0703081;
S. Argyropoulos, T. Sjöstrand, J. High Energy Phys. 1411 (2014) 043, arXiv:1407.6653 [hep-ph].
[22] H. Paukkunen, C.A. Salgado, Phys. Rev. Lett. 110 (21) (2013) 212301, arXiv:1302.2001 [hep-ph].
[23] H. Paukkunen, P. Zurita, J. High Energy Phys. 1412 (2014) 100, arXiv:1402.6623 [hep-ph].
[24] H.-L. Lai, et al., Phys. Rev. D 82 (2010) 074024, arXiv:1007.2241 [hep-ph].
[25] M. Arneodo, Phys. Rep. 240 (1994) 301.
[26] K.J. Eskola, H. Paukkunen, C.A. Salgado, J. High Energy Phys. 0904 (2009) 065, arXiv:0902.4154 [hep-ph].
[27] M. Hirai, S. Kumano, T.-H. Nagai, Phys. Rev. C 76 (2007) 065207, arXiv:0709.3038 [hep-ph].
[28] I. Schienbein, et al., Phys. Rev. D 80 (2009) 094004, arXiv:0907.2357 [hep-ph].
[29] D. de Florian, R. Sassot, P. Zurita, M. Stratmann, Phys. Rev. D 85 (2012) 074028, arXiv:1112.6324 [hep-ph].
[30] S. Chatrchyan, et al., CMS Collaboration, Eur. Phys. J. C 74 (2014) 2951, arXiv:1401.4433 [nucl-ex].
[31] H. Paukkunen, K.J. Eskola, C. Salgado, arXiv:1408.4563 [hep-ph].
[32] A. Kusina, et al., PoS DIS 2014 (2014) 047, arXiv:1408.1114 [hep-ph].
[33] J.M. Campbell, F. Tramontano, Nucl. Phys. B 726 (2005) 109, arXiv:hep-ph/0506289.
[34] V. Khachatryan, et al., CMS Collaboration, Phys. Lett. B 695 (2011) 424, arXiv:1010.5994 [hep-ex].
[35] S. Chatrchyan, et al., CMS Collaboration, J. High Energy Phys. 1107 (2011) 049, arXiv:1105.5661 [hep-ex].
[36] S. Chatrchyan, et al., CMS Collaboration, Eur. Phys. J. C 71 (2011) 1721, arXiv:1106.0902 [hep-ex].
[37] S. Chatrchyan, et al., CMS Collaboration, Phys. Rev. D 85 (2012) 112007, arXiv:1203.6810 [hep-ex].
[38] S. Chatrchyan, et al., CMS Collaboration, J. High Energy Phys. 1211 (2012) 067, arXiv:1208.2671 [hep-ex].
[39] S. Chatrchyan, et al., CMS Collaboration, Eur. Phys. J. C 73 (2013) 2339, arXiv:1211.2220 [hep-ex].
[40] S. Chatrchyan, et al., CMS Collaboration, Eur. Phys. J. C 73 (2013) 2386, arXiv:1301.5755 [hep-ex].
[41] S. Chatrchyan, et al., CMS Collaboration, J. High Energy Phys. 1402 (2014) 024, Erratum: J. High Energy Phys. 1402 (2014) 102, arXiv:1312.7582 [hep-ex].
[42] G. Aad, et al., ATLAS Collaboration, Eur. Phys. J. C 71 (2011) 1577, arXiv:1012.1792 [hep-ex].
[43] G. Aad, et al., ATLAS Collaboration, Phys. Lett. B 707 (2012) 459, arXiv:1108.3699 [hep-ex].
[44] G. Aad, et al., ATLAS Collaboration, Phys. Lett. B 711 (2012) 244, arXiv:1201.1889 [hep-ex].
[45] G. Aad, et al., ATLAS Collaboration, J. High Energy Phys. 1205 (2012) 059, arXiv:1202.4892 [hep-ex].
[46] V. Khachatryan, et al., CMS Collaboration, J. High Energy Phys. 1406 (2014) 090, arXiv:1403.7366 [hep-ex].
[47] G. Aad, et al., ATLAS Collaboration, Phys. Lett. B 717 (2012) 89, arXiv:1205.2067 [hep-ex].
[48] G. Aad, et al., ATLAS Collaboration, Eur. Phys. J. C 73 (1) (2013) 2261, arXiv:1207.5644 [hep-ex].
[49] S. Chatrchyan, et al., CMS Collaboration, Phys. Rev. Lett. 107 (2011) 091802, arXiv:1106.3052 [hep-ex].
[50] S. Chatrchyan, et al., CMS Collaboration, J. High Energy Phys. 1212 (2012) 035, arXiv:1209.4533 [hep-ex].
[51] G. Aad, et al., ATLAS Collaboration, Phys. Lett. B 717 (2012) 330, arXiv:1205.3130 [hep-ex].
[52] G. Aad, et al., ATLAS Collaboration, Phys. Rev. D 90 (2014) 112006, arXiv:1406.7844 [hep-ex].
[53] S. Chatrchyan, et al., CMS Collaboration, Phys. Rev. Lett. 110 (2013) 022003, arXiv:1209.3489 [hep-ex].
[54] S. Chatrchyan, et al., CMS Collaboration, Phys. Rev. Lett. 112 (2014) 231802, arXiv:1401.2942 [hep-ex].
[55] G. Aad, et al., ATLAS Collaboration, Phys. Lett. B 716 (2012) 142, arXiv:1205.5764 [hep-ex].
[56] K.J. Eskola, Nucl. Phys. A 910–911 (2013) 163, arXiv:1209.1546 [hep-ph].
[57] V. Khachatryan, et al., CMS Collaboration, Heavy ions projections at HL-LHC, CMS-PAS-FTR-13-025, 2013.
[58] M. Cacciari, G.P. Salam, G. Soyez, J. High Energy Phys. 0804 (2008) 063, arXiv:0802.1189 [hep-ph].
[59] J. Pumplin, et al., Phys. Rev. D 65 (2001) 014013, arXiv:hep-ph/0101032.
[60] W.T. Giele, S. Keller, Phys. Rev. D 58 (1998) 094023, arXiv:hep-ph/9803393.
[61] N. Sato, J.F. Owens, H. Prosper, Phys. Rev. D 89 (2014) 114020, arXiv:1310.1089 [hep-ph].
[62] M.L. Mangano, J. Rojo, J. High Energy Phys. 1208 (2012) 010, arXiv:1206.3557 [hep-ph].
[63] S. Albino, B.A. Kniehl, G. Kramer, Nucl. Phys. B 803 (2008) 42, arXiv:0803.2768 [hep-ph].
[64] S.S. Adler, et al., PHENIX Collaboration, Phys. Rev. Lett. 98 (2007) 172302, arXiv:nucl-ex/0610036.